

Intended for the Astrophysical Journal, Supplement Series

## Integrated Polarization Properties of 3C48, 3C138, 3C147, and 3C286

R. A. Perley and B. J. Butler

RPerley@nrao.edu, BButler@nrao.edu

*National Radio Astronomy Observatory<sup>1</sup>*

*P.O.Box O, Socorro, NM, 87801*

### ABSTRACT

We present the integrated polarization properties of the four compact radio sources 3C48, 3C138, 3C147 and 3C286, from 1 to 50 GHz, over a 30-year time frame spanning 1982 to 2012. These four sources are commonly used as flux density and polarization calibrators for cm-wave interferometers. Using the polarized emission of Mars, we have determined that the true position angle of the linearly polarized emission of 3C286 rises from 33 degrees at 8 GHz to 36 degrees at 45 GHz. There is no evidence for a change in the position angle over time. Using these values, the position angles of the integrated polarized emission from the other sources are determined as a function of frequency and time. The fractional polarization of 3C286 is found to be slowly rising, at all frequencies, at a rate of  $\sim 0.015\%$ /year. The fractional polarizations of 3C48, 3C138, and 3C147 are all slowly variable, with the variations clearly correlated with changes in the total flux densities of these sources.

*Subject headings:* Instrumentation:interferometers, Methods: data analysis, observational, Techniques: interferometric, Telescopes(VLA)

---

<sup>1</sup>The National Radio Astronomy Observatory is a facility of the National Science Foundation operated under cooperative agreement by Associated Universities, Inc.

## 1. Introduction

Perley and Butler (2013) have proposed an absolute spectral flux density scale valid from 1 to 50 GHz, based on the known absolute emission spectrum from the planet Mars (Weiland *et al.* (2011)), and employing accurate flux density ratios derived by the VLA approximately yearly since 1983. They propose that the quasar 3C286, whose flux density has been stable to  $\sim 1\%$  over the past 30 years, be employed as the primary flux density calibrator source for frequencies between 1 through 50 GHz, and provide a polynomial expression for its spectral flux density. In addition, Perley and Butler (2013) provide time-variable polynomial expressions for the spectral flux densities of 3C48, 3C138, and 3C147.

The VLA, prior to its upgrade, always provided full polarization information when used in its standard continuum operating modes. The nineteen separate observing sessions utilized by Perley and Butler (2013) provides a detailed database from which the polarization properties of the fourteen target sources can be determined. In addition, since the planet Mars was extensively observed in this program, its well known polarization characteristics can be utilized to establish the true position angle of polarized emission of the other sources.

In this paper, we briefly describe the polarization calibration procedure, and give results for the integrated polarization properties of the four most compact sources in the program – 3C48, 3C138, 3C147, and 3C286.

## 2. Polarization Calibration

### 2.1. Observing Methodology and Calibration

The observing methodology and calibration procedures are described in detail in Perley and Butler (2013), and will not be repeated here. The additional calibration steps employed to determine the antenna polarization, and the position angle of linearly polarized flux density are given below.

- The position angle rotation introduced by the earth’s ionosphere was estimated by utilizing TEC data from the CDDIS data archive with a model of the earth’s magnetic field. The predicted corresponding phase rotation was applied to the LCP data. The correction is typically a few degrees at 1.5 GHz, and is unimportant above  $\sim 5$  GHz.
- The antenna polarizations were measured utilizing the technique of Conway and Kronberg (1969) which utilizes the rotation of the antenna parallactic angle,  $\Psi$ , over time. This

rotation permits a separation of the antenna from the source polarizations, and provides estimates of each.

- The plane of linear polarization was based initially by adjusting the phase of the LCP channel so the observed position angle of the polarized flux density from 3C286 was 33 degrees at all frequencies.

Following this calibration procedure, images for all sources in Stokes parameters Q and U were made for each epoch. The polarized images of the optically thin unpolarized source NGC7027 demonstrate the accuracy of our determinations of the fractional polarization to be typically 0.1%.

Our observing program comprised fourteen sources, observed at all VLA frequency bands in the lowest-resolution ‘D’ configuration. The polarization imaging results for the heavily resolved sources 3C123, 3C196, and 3C295 show a complicated polarization pattern, with very low integrated polarization. Because of this, these sources are not useful as polarization calibrators. No linear polarization, to a limit  $\sim 0.1\%$ , was found for the planetary nebulae NGC7027 and NGC6572, the evolved star MWC349, and the planets Uranus and Neptune. Venus does show some polarization from its surface at low frequencies, but the quality of the data and the resolution of the images are both too low for these results to be useful.

The sources 3C48, 3C138, 3C147, and 3C286 are all significantly polarized at most frequencies utilized by the VLA. All are very compact, and are thus useful for polarization calibration purposes, providing their integrated polarization properties are at most slowly variable. The planet Mars was sufficiently resolved on twelve observing sessions at our higher frequencies that its polarization can be imaged and utilized to calibrate the position angle for the other sources. The procedure is described in the following section.

### 3. The True Position Angle for the Polarized Flux of 3C286

Most VLA users have adopted the value of 33 degrees for the position angle of the linearly polarized flux density of 3C286 at all frequencies. This value was determined by Bignell and Seaquist (1973) with a quoted error of  $\pm 0.9$  degrees, and is based on observations at 6.7 GHz with the Algonquin Radio Telescope. Bignell and Seaquist (1973) also give a position angle of  $31 \pm 1.3$  degrees for 3C286 at 10.7 GHz. We are not aware of any systematic effort to measure the true position angle of 3C286 at other frequencies in order to check the common assumption that the position angle is independent of wavelength. Our

observations of Mars provide the capability to make this check for the higher frequencies where we are able to resolve the planet’s disk, as the emission of blackbody radiation from a planet such as Mars will show a radially oriented linear polarization which maximizes near the limb of the planet (Heiles and Drake (1963)).

For a solid body such as Mars, the thermal radio emission originates from beneath the surface, which upon crossing the surface, is refracted according to Snell’s law

$$\sin \theta_t = \frac{n_i}{n_t} \sin \theta_i, \quad (1)$$

where  $\theta$  is the propagation angle with respect to the surface normal,  $n = \sqrt{\epsilon}$  is the index of refraction,  $\epsilon$  is the dielectric constant for the particular medium, and the subscripts  $i$  and  $t$  represent the media for the incident and transmitted radiation. (We assume non-magnetic media, for which  $\mu = 1$ ). Because of the change in media properties at the planetary surface, from  $n_i > 1$  to  $n_t \sim 1$ , part of the emerging wave is reflected, and part transmitted. The fraction transmitted depends upon the angle of incidence, the dielectric constant, and the polarization. The transmissivity (defined as the fraction of the incident power which is transmitted across the boundary) is given by Born and Wolf (1980)

$$T_{\parallel} = \frac{\sin 2\theta_i \sin 2\theta_t}{\sin^2(\theta_i + \theta_t) \cos^2(\theta_i - \theta_t)} \quad (2)$$

$$T_{\perp} = \frac{\sin 2\theta_i \sin 2\theta_t}{\sin^2(\theta_i + \theta_t)}. \quad (3)$$

The parallel linear polarization component lies in the plane defined by the incident and transmitted propagation directions. The perpendicular component is orthogonal to this plane.

Assuming a simple model where Mars is a uniform sphere of radius  $R$ , the radiation emitted towards the observer from a location with perpendicular offset  $d$  from the center of the visible disk leaves the planet surface at angle  $\sin(\theta) = d/R$  to the local planet normal. Defining  $x = d/R$  as the fractional perpendicular offset from the planet center, the transmissivity can be written, using equations (1), (2), and (3) as

$$T_{\parallel}(x) = \frac{4\epsilon\sqrt{1-x^2}\sqrt{\epsilon-x^2}}{(\epsilon\sqrt{1-x^2} + \sqrt{\epsilon-x^2})^2} \quad (4)$$

$$T_{\perp}(x) = \frac{4\sqrt{1-x^2}\sqrt{\epsilon-x^2}}{(\sqrt{1-x^2} + \sqrt{\epsilon-x^2})^2}. \quad (5)$$

The parallel component is radially oriented, and the perpendicular component is azimuthally oriented. It can be shown that  $T_{\parallel} > T_{\perp}$  for  $0 < x < 1$ . Further,  $T_{\parallel}$  rises from the planet

center outwards, reaches a maximum of unity at the Brewster angle,  $x = \sqrt{\epsilon/(1 + \epsilon)}$ , and falls dramatically thereafter, while  $T_{\perp}$  declines uniformly with offset. Hence, the observed emission will be radially polarized, with the fractional polarization increasing with offset. The fractional degree of polarization

$$p = \frac{T_{\parallel}(x) - T_{\perp}(x)}{T_{\parallel}(x) + T_{\perp}(x)} \quad (6)$$

is a strong function of the planet dielectric constant  $\epsilon$ , rising from zero at the planet center to a maximum very near to the planet’s limb (Heiles and Drake (1963)). For Mars, with  $\epsilon \sim 2.5$  (Rudy *et al.* (1987)), the maximum linear polarization would exceed 30%, were the Martian surface smooth.

Finite angular resolution and surface roughness will reduce the observed fractional polarization (Hagfors and Moriello (1965), Alekseev *et al.* (1968), Golden (1979)), but the radial position angle relation will be preserved on large scales, allowing a position angle calibration to be established for observations which adequately resolve the planet’s disk.

To illustrate this effect, we show in Fig. 1 images of the polarized intensity, and the position angle of the polarized intensity at 43 GHz, taken from our observations on April 16, 1999, when Mars had an angular diameter of 15.6 arcseconds. The instrumental resolution is 2.0 arcseconds.

Twelve of the thirteen observing sessions which included the planet Mars were taken when Mars had an angular diameter sufficiently large to resolve its polarization in at least one frequency band. For these sessions, we made polarization images of Mars at all frequencies where there were at least three resolution elements across the planet. The lowest frequency at which this could be done for our observations was 5 GHz. A special AIPS task was written to find the mean deviation of the observed position angle around the planet’s disk from the radial direction. This deviation was then added to the assumed value of 33 degrees for 3C286 to determine the correct position angle for that source. The measured position angles for the remaining sources were subsequently corrected using this offset. The observed deviations, and (1- $\sigma$ ) error are given in Table 1. The bottom line in Table 1 gives the weighted mean of the data and the probable error. A small but significant offset is found. The corrected values for 3C286 are given in Table 2.

### 3.1. Polarization Properties for the Four Primary Calibrators

In Table 3 we show the fractional linear polarizations, and the position angles of the polarized intensity from the four compact sources, taken from the observation run of December

Table 1. Offset Angles from  $33^\circ$  of Mars’ Polarized Emission

Session	3 cm	2 cm	1.3 cm	1.0 cm	0.7 cm
1995			-2.5±0.6		
1999	-1.0±1.8	-0.5±1.0	-2.9±1.0		-4.4±0.5
2000					-3.5±5.1
2001		-0.7±7.0	-3.1±3.2		-2.2±4.3
2003			-0.4±4.0		-3.7±2.5
2004					2.3±3.5
2006		-0.3±2.4	-3.2±1.1		-0.5±1.2
2007			2.0±8.8		0.4±3.7
2008					0.5±3.8
2010	-0.6±4.3		-1.5±1.2	-2.6±1.1	-4.4±0.5
	0.7±4.0		-1.3±1.6	1.9±1.4	
2011		-1.8±3.2	-1.6±2.2	1.7±2.0	0.5±3.6
			-1.9±3.9	3.9±1.3	
2012	0.6±3.9	-3.5±1.3	0.4±0.8	-4.1±1.0	-2.6±0.9
	0.5±2.9	-1.2±1.5	-2.3±0.8	-4.5±0.8	-3.3±0.6
Wgt.Mean	-0.3±0.9	-1.6±0.3	-1.91±0.12	-2.50±0.33	-2.77±0.10

Note. — The last line gives the weighted mean of the tabular entries for each wavelength band. The listed error is the weighted ( $1-\sigma$ ) error.

Table 2. The True Polarization Position Angle for 3C286

P.A.	5 GHz	15 GHz	23 GHz	33 GHz	45 GHz
3C286	33± 1	34.5±0.5	35±0.2	35.5±0.4	35.8±0.1

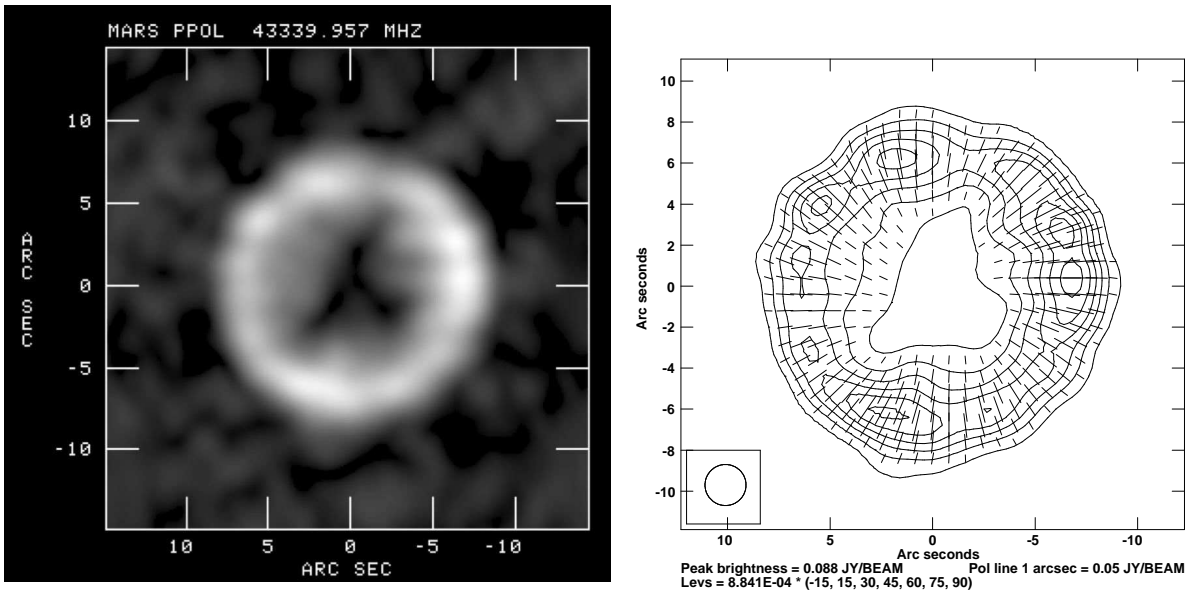


Fig. 1.— (Left) A grey-scale image of the linearly polarized intensity from Mars, with resolution 2 arcseconds, on 16 April, 1999. The planet diameter is 15.6 arcseconds. (Right) A contour plot of the same image, with the apparent position angle of polarized flux density superposed. A small deviation from purely radial is apparent.

2010. The position angles are referenced to 3C286, which was set to 33 degrees for frequencies between 1 and 8 GHz, and to the angles given in Table 2 for higher frequencies. These same data, in graphical form, are shown in Fig. 2, following adjustment for the rotation measure. In this figure, the position angle data for 3C147 at frequencies less than 7 GHz are not shown, as the source is too heavily depolarized to allow a meaningful determination of the position angle.

The position angle of the linearly polarized flux density changes rapidly with wavelength for 3C48 and 3C147. For both, the relationships are well fitted by a  $\lambda^2$  law:  $\chi(\lambda) = (RM)\lambda^2 + \chi_0$ , over part of the frequency range spanned by our observations. We made a least squares fit to this function for all four sources, with the results given in Table 4.

Of interest is any variation in the polarization properties of these sources over time. The recent outburst in 3C138 and the smaller changes in 3C48 and 3C147 (see Perley and Butler (2013)) may be expected to result in changes in polarization, as the polarized emission from the emerging component may not align with that from the larger-scale, older emission. Shown in Fig. 3 is the temporal variation in the fractional polarization and in the position angles of the four primary calibration sources since 1983. The figure shows that the fractional polarization of 3C48 has undergone a small but notable rise since this monitoring program

Table 3. Polarization Properties of 3C48, 3C138, 3C147, and 3C286

Freq. GHz	3C48p %	3C48 $\chi$ deg.	3C138p %	3C138 $\chi$ deg.	3C147p %	3C147 $\chi$ deg.	3C286p %	3C286 $\chi$ deg.
1.050	0.3	25	5.6	-14	< .05	–	8.6	33
1.450	0.5	140	7.5	-11	< .05	–	9.5	33
1.640	0.7	-5	8.4	-10	< .04	–	9.9	33
1.950	0.9	-150	9.0	-10	< .04	–	10.1	33
2.450	1.4	-120	10.4	-9	< .05	–	10.5	33
2.950	2.0	-100	10.7	-10	< .05	–	10.8	33
3.250	2.5	-92	10.0	-10	< .05	–	10.9	33
3.750	3.2	-84	–	–	< .04	–	11.1	33
4.500	3.8	-75	10.0	-11	0.1	-100	11.3	33
5.000	4.2	-72	10.4	-11	0.3	0	11.4	33
6.500	5.2	-68	9.8	-12	0.3	-65	11.6	33
7.250	5.2	-67	10.0	-12	0.6	-39	11.7	33
8.100	5.3	-64	10.4	-10	0.7	-24	11.9	33
8.800	5.4	-62	10.1	-8	0.8	-11	11.9	33
12.80	6.0	-62	8.4	-7	2.2	43	11.9	34
13.70	6.1	-62	7.9	-7	2.4	48	11.9	34
14.60	6.4	-63	7.7	-8	2.7	53	12.1	34
15.50	6.4	-64	7.4	-9	2.9	59	12.2	34
18.10	6.9	-66	6.7	-12	3.4	67	12.5	34
19.00	7.1	-67	6.5	-13	3.5	68	12.5	35
22.40	7.7	-70	6.7	-16	3.8	75	12.6	35
23.30	7.8	-70	6.6	-17	3.8	76	12.6	35
36.50	7.4	-77	6.6	-24	4.4	85	13.1	36
43.50	7.5	-85	6.5	-27	5.2	86	13.2	36

Note. — isted are the properties as measured in December 2010. The polarization of 3C138 has been changing at the higher frequencies due to a large flare which began in 2003. The other sources show relatively stable polarization over time.

Table 4. RM Values for the Four Sources

Source	Wavelength Range cm	RM rad/m <sup>2</sup>	$\chi_0$ deg.
3C48	1 – 18	-68	122
3C138	2 – 22	0	-10
3C147	1 – 3	-1467	88
3C286	1 – > 30	0	33



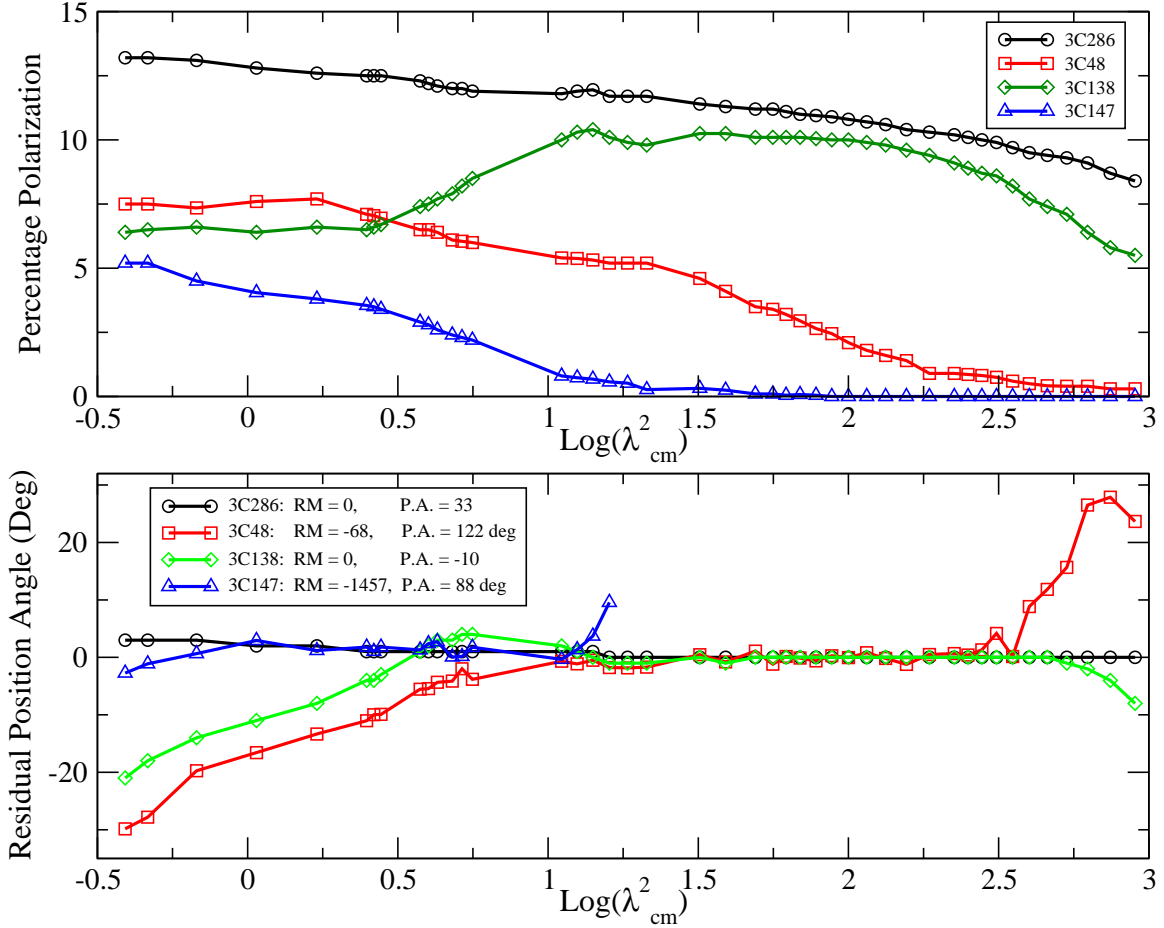


Fig. 2.— The fractional polarization, and the position angle, for the four primary calibrators, as a function of frequency. These data are from the Dec 2010 session. Note that the RM values shown in the lower frame have been used to unwrap the position angles.

began, although there appears to be no effect in the position angle. As expected, there was a dramatic change in the polarization properties in 3C138 at higher frequencies, beginning in 2003, when the flare began. With the flare intensity now waning, the polarization properties appear to be returning to the same values noted before 2003. The flux density changes noted for 3C147 are accompanied by small changes in its polarization, particularly at higher frequencies. The fractional polarization of 3C286 appears to be slowly, and steadily rising over the period. A simple linear fit to the data provides the values shown in Table 5, giving the fractional polarization in percent for epoch 2000.0, and its change in percent/century.

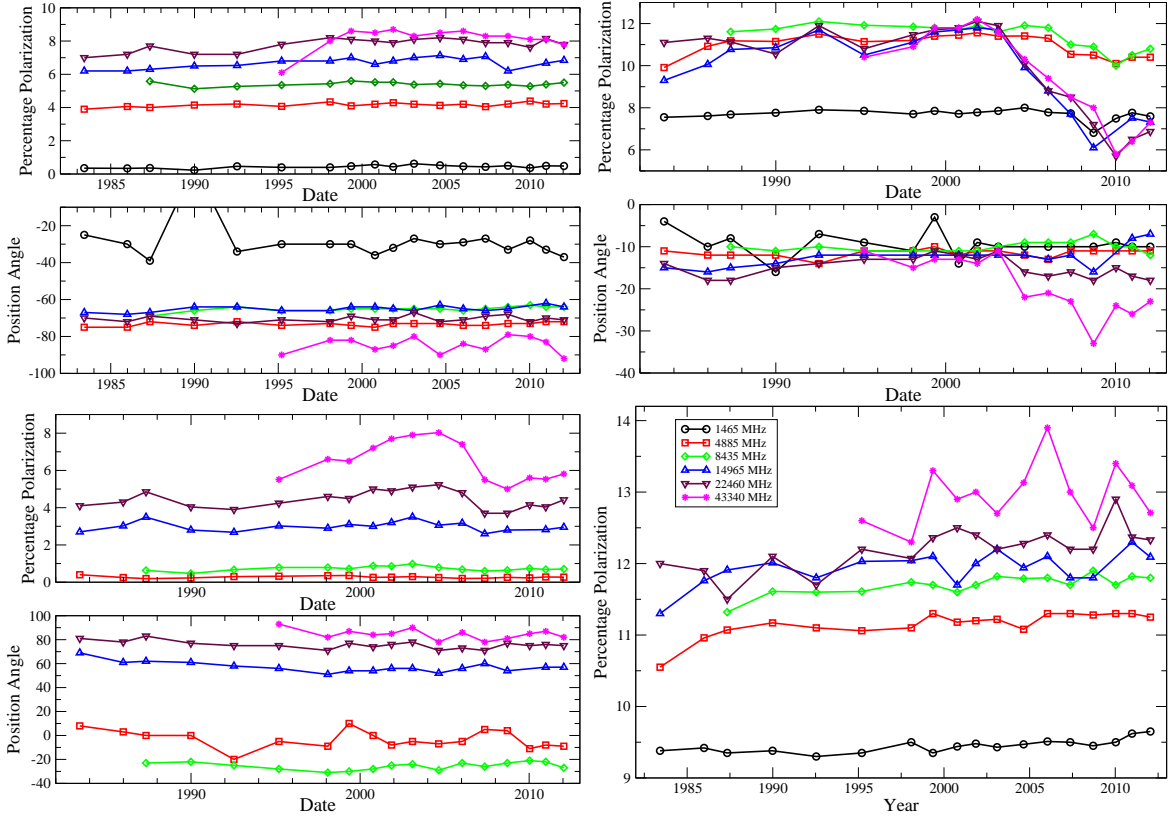


Fig. 3.— The percentage polarization, and the polarization position angle for 3C48 (upper left), 3C138 (upper right), 3C147 (lower left), and 3C286 (lower right, fractional polarization only).

## 4. Discussion

All four sources have been extensively observed with the VLBA, MERLIN, and EVN. Here we briefly compare the polarimetric results from these instruments against our own.

### 4.1. 3C48

The source was the subject of an extensive study by An *et al.* (2010), utilizing the VLBA, MERLIN, and the EVN. Their paper shows that the emission from 3C48 on milliarcsecond scales is quite complicated, with a short and twisted jet-like structure blending into an extended region located to the NE of the quasar core. Our global rotation measure value of  $-68 \text{ rad/m}^2$  is in good agreement with the ‘spot’ values from their component ‘C’ of  $-68$  to  $-95 \text{ rad/m}^2$ . The MERLIN polarimetric image at 1.65 GHz shows the weak po-

larized emission aligned nearly vertically, in good agreement with our integrated value of -5 degrees at 1.64 GHz. The heavily resolved VLBA images shown in their Figure 6 at 4.78 and 8.31 GHz are difficult to compare to our integrated values, but the polarized position angles shown are close to our integrated values. High resolution VLA images taken at 26 GHz with 70 mas resolution show the majority of the polarized emission coming from bright northern component labelled ‘C’ in An *et al.* (2010), with the more compact structures labeled by them at ‘B’, ‘B2’, and ‘B3’.

## 4.2. 3C138

The small-scale structure is shown in Cotton *et al.* (1997a) to comprise a relative weak unresolved nuclear core, a strong and well-resolved jet-like structure extending  $\sim 400$  milliarcseconds to the NE, and a very weak counter-jet 250 milliarcseconds to the SW. The NE jet is highly and uniformly polarized, and accounts for nearly all the total polarized emission seen in our integrated measures. Their Figure 4 shows the weaker, trailing parts of the NE jet to have a linearly polarized emission at p.a.  $\sim -25$  degrees, while the much brighter head of the jet to have its polarized emission at an angle near 0. The sum of the two components is near our integrated measure of  $\sim -10$  degrees. Our data show the position angle to decrease by about 15 degrees as the frequency rises – this is probably due to a spectral index effect whereby the head of the NE jet becomes more prominent compared to the steeper spectrum trailing areas. The decline in integrated polarization, and decrease in the resulting position angle, seen since 2002 at the higher frequencies are likely due to an emerging new component along p.a. near -30 (as shown in Figure 6 in Cotton *et al.* (1997a)) with polarization along this angle.

Table 5. Change in Fractional Polarization of 3C286

Freq. GHz	P(2000) %	Slope %/century
1.465	$9.450 \pm .015$	$0.77 \pm 0.17$
4.885	$11.18 \pm .02$	$1.0 \pm 0.2$
8.435	$11.67 \pm .02$	$1.4 \pm 0.3$
14.965	$11.97 \pm .04$	$0.8 \pm 0.5$
22.485	$12.20 \pm .05$	$2.5 \pm 0.6$
43.340	$12.87 \pm .16$	$2.2 \pm 2.3$

### 4.3. 3C147

VLBA polarimetric imaging at 5 and 8 GHz for 3C147 has been presented by Rossetti *et al.* (2009). At milliarcsecond resolution, the source comprises a compact core and apparently rapidly expanding jet, extending only  $\sim 10$  milliarcseconds to the SW. Beyond this, a very diffuse and well-resolved lobe extends to the SW to a maximum extent of  $\sim 180$  milliarcseconds. High resolution VLA observations at  $\sim 70$  milliarcseconds resolution show another, more extended and detached elongated lobe extending northwards  $\sim 700$  milliarcseconds. 3C147 has an extremely high RM of  $-1467 \text{ rad/m}^2$ , in good agreement with the value reported by Rossetti *et al.* (2009) for their component B, located at the end of the inner, flaring jet. High resolution VLA polarimetric imaging at 25 GHz with 70 milliarcsecond resolution shows that the nucleus and inner jet regions dominate the total polarized flux density. The true integrated position angle of 88 degrees from our integrated measures agrees well with the intrinsic angle for the B-field of the flaring jet shown by Rossetti *et al.* (2009) in their Figure 7.

### 4.4. 3C286

The quasar 3C286 was selected by Perley and Butler (2013) as the primary non-variable flux density standard from 1 to 50 GHz, based on the stability of its total intensity over period exceeding 30-years. This current study shows that 3C286 also serves as an equally useful and stable reference source for polarimetry. Although we detect a very small secular increase in its polarized flux density, the change appears to be steady, permitting easy calculation of the expected polarized flux density at any epoch.

High resolution polarimetry of this source is shown by Jiang *et al.* (1996) and Cotton *et al.* (1997b). The latter paper sketches the overall structure, comprising a central core, a compact eastern lobe about 1 arcsecond east, and an extended western lobe, extending  $\sim 2.5$  arcseconds to the SE. The central core region contains a highly polarized extension of length  $\sim 80$  milliarcseconds, in p.a. 135 degrees – i.e., pointing towards the SE lobe. Both the total and polarized emission from this source are unusual. There is no clearly defined inverted spectrum core, suggesting either a dearth of recent activity, or a geometry whereby the core emission is beamed away from our direction. The polarized emission is almost entirely along the jet, contrary to the general rule where jet emission is primarily polarized transversely to the jet axis.

3C286 has recently been proposed by Agudo *et al.* (2012) as a polarization calibration source for millimeter-wavelength observations. Their results are in excellent agreement with

a simple extrapolation of ours: a polarization fraction of 13.5% and an intrinsic position angle of 37.4 degrees at  $\lambda = 3$  mm. Agudo *et al.* (2012) also provide values at  $\lambda = 1$  mm of 14.5% and 33.5 degrees – however, these have much larger error estimates, and are not inconsistent with our results.

## 5. Summary

We have determined that the position angle of linearly polarized emission from 3C286 rises from 33 degrees at frequencies below 10 GHz, to 36 degrees at 43 GHz. Changes in this position angle over time are less than  $\sim 2$  degrees over the past 20 years. The fractional linear polarization of 3C286 is steadily increasing at all frequencies at a rate of about 0.15%/year.

The polarization characteristics of 3C48 and 3C147 are fairly stable, but small changes, likely related to the small variations in total intensity noted by Perley and Butler (2013) are visible. The polarization position angles for these two objects for frequencies at which their fractional polarization exceed 1% are well fitted with a simple  $\lambda^2$  law over most of the observed frequency range.

The strongly polarized source 3C138 has undergone a notable flare, beginning in 2003, which nearly doubled its total intensity by 2010, and has been rapidly declining since. The polarization properties also changed dramatically during this period, and appear to be returning to the pre-flare levels.

## 6. Acknowledgement

We thank Eric Greisen for generating the special AIPS task to calculate the mean offset in polarization position angle.

## REFERENCES

- Agudo, I., Thum, C., Wiesemeyer, H., *et al.* 2012 A&A, 541, A111
- Alekseev, V.A., Aleshina, V.D., Krotikov, V.D., and Troitskii, V.S. 1968, Sov. Astron., 11, 860
- An, T., Hong, X.Y., Hardcastle, M.J., *et al.* 2010, MNRAS, 402, 87
- Baars, J.W.M., Genzel, R., Pauliny-Toth, I.K.K., and Witzel, A. 1977, A&A, 61, 99

- Bignell, R.C., and Seaquist, E.R. 1973, *AJ*, 78, 536
- Born, Max, and Wolf, Emil 1980 *Principles of Optics*, Sixth Edition, Section 1.5.3
- Conway, R.G., and Kronberg, P.P. 1969, *MNRAS*, 142, 11
- Cotton, W.D., Dallacasa, D., Fanti, C., *et al.* 1997, *A&A*, 325, 493
- Cotton, W.D., Fanti, C., Fanti, R., *et al.* 1997, *A&A*, 325, 479
- Hagfors, T., and Moriello, J., 1965, *Radio Science*, 69, 1614
- Heiles, C.E., and Drake, F.D., *Icarus*, 2, 281
- Golden, L.M. *Icarus*, 38, 451
- Jiang, D.R., Dallacasa, D., Schilizzi, R.T., *et al.*, *A&A*, 312, 380
- Perley, R.A., and Butler, B.J. Accepted by *ApJS*
- Rossetti, A., Mantovani, F., Dallascasa, D. *et al.*, *A&A*, 504, 741
- Rudy, D.J., Muhleman, D.O., Berge, G.L., *et al.* *Icarus*, 71, 159
- Weiland, J.L., Odegard, N., Hill, R.S., *et al.* 2011, *ApJS*, 192,1